Human IAPP–induced pancreatic β cell toxicity and its regulation by autophagy

Nayumi Shigihara,[1,2] Ayako Fukunaka,[1,2] Akemi Hara,[2,3] Koji Komiya,[1,2] Akira Honda,[1,2] Toyoyoshi Uchida,[1] Hiroko Abe,[1] Yukiko Toyofuku,[1] Motoyuki Tamaki,[1] Takeshi Ogihara,[1] Takeshi Miyatsuka,[1,4] Henry J. Hiddinga,[5] Setsuya Sakagashira,[5] Masato Koike,[6] Yasuo Uchiyama,[6] Tamotsu Yoshimori,[2,7] Norman L. Eberhardt,[5] Yoshio Fujitani,[1,2,3] and Hirotaka Watada[1,3,4,8,9]

[1]Department of Metabolism and Endocrinology, [2]JST-CREST Program, [3]Center for Beta-Cell Biology and Regeneration, and [4]Center for Molecular Diabetology, Juntendo University Graduate School of Medicine, Tokyo, Japan. [5]Division of Endocrinology, Department of Medicine, Mayo Clinic, Rochester, Minnesota, USA. [6]Department of Cell Biology and Neuroscience, Juntendo University Graduate School of Medicine, Tokyo, Japan. [7]Department of Genetics, Graduate School of Medicine, Osaka University, Suita, Japan. [8]Sportology Center and [9]Center for Therapeutic Innovations in Diabetes, Juntendo University Graduate School of Medicine, Tokyo, Japan.

Pancreatic islets in patients with type 2 diabetes mellitus (T2DM) are characterized by loss of β cells and formation of amyloid deposits derived from islet amyloid polypeptide (IAPP). Here we demonstrated that treatment of INS-1 cells with human IAPP (hIAPP) enhances cell death, inhibits cytoproliferation, and increases autophagosome formation. Furthermore, inhibition of autophagy increased the vulnerability of β cells to the cytotoxic effects of hIAPP. Based on these in vitro findings, we examined the pathogenic role of hIAPP and its relation to autophagy in hIAPP-knockin mice. In animals fed a standard diet, hIAPP had no toxic effects on β cell function; however, hIAPP-knockin mice did not exhibit a high-fat-diet–induced compensatory increase in β cell mass, which was due to limited β cell proliferation and enhanced β cell apoptosis. Importantly, expression of hIAPP in mice with a β cell–specific autophagy defect resulted in substantial deterioration of glucose tolerance and dispersed cytoplasmic expression of p62-associated toxic oligomers, which were otherwise sequestrated within p62-positive inclusions. Together, our results indicate that increased insulin resistance in combination with reduced autophagy may enhance the toxic potential of hIAPP and enhance β cell dysfunction and progression of T2DM.

Introduction

Type 2 diabetes mellitus (T2DM) is characterized by insulin resistance and β cell failure (1); the latter is caused by reduction in β cell function (2, 3) and β cell mass (4–6). One of the characteristic morphological changes in pancreatic islets of human T2DM is amyloid deposition (7–9). Pancreatic islet amyloid is found in approximately 90% of patients with T2DM, and the extent of its deposition correlates negatively with β cell mass (8). The major constituent of islet amyloid in humans is derived from islet amyloid polypeptide (IAPP; also known as amylin), a 37–amino acid polypeptide synthesized in pancreatic β cells and coreleased with insulin in response to a rise in blood glucose level (8, 10). IAPP exhibits close amino acid homology in the N- and C-terminal regions in all species studied (9, 11). In addition, the 20–29 region is homologous among humans, cats, and monkeys and is hydrophobic and amyloidogenic (8, 9, 11). In contrast, in mouse IAPP, the 20–29 region has proline substitutions compared with human IAPP (hIAPP), and, as a result, mouse IAPP is soluble and nonamyloidogenic (8, 9, 11, 12). Rodent IAPP, which lacks β sheet structure, does not form aggregates, and thus the commonly used rodent models of diabetes do not recapitulate islet pathology in humans. To investigate the role of hIAPP, several mouse models and a rat model transgenic for hIAPP have been developed (13–16). Studies in these models have shown that overexpression of hIAPP exhibits toxic effects on β cells by inducing apoptosis and amyloidogenesis in a context-dependent manner. However, these traditional transgenic approaches resulted in large phenotypic variations, presumably due to multiple copy insertions that affect the expression levels and integration of genes near other transcriptional control elements that can adversely modulate expression (17). Expression of hIAPP driven by rat insulin promoter (RIP) is expected to be largely different from that regulated by the endogenous murine *Iapp* gene. To minimize these variations and explore the physiological roles of hIAPP in β cell deficit, a knockin mouse was generated in which the endogenous murine *Iapp* coding region was genetically replaced with that of *hIAPP* (17). In contrast to the results obtained by in vitro overexpression and transgenic overexpression of hIAPP (15, 18, 19), expression of WT hIAPP in the knockin mouse model failed to induce islet amyloid formation; rather, it induced mild glucose intolerance (17), which suggests that hIAPP-knockin mice represent a useful model for pathogenic characterization of hIAPP in a physiological setting.

▶ Related Commentary: p. 3292

Authorship note: Nayumi Shigihara, Ayako Fukunaka, Akemi Hara, and Yoshio Fujitani contributed equally to this work.
Conflict of interest: Yoshio Fujitani has received lecture fees from Novartis and Eli Lilly and research funding from MSD, Eli Lilly, and Takeda. Hirotaka Watada has received lecture fees from Daiichi Sankyo, Takeda, MSD, Sanofi-Aventis, Ono, Novartis, Astellas, Dainippon Sumitomo, Tanabe Mitsubishi, Novo Nordisk, and Sanwakagaku and research funding from Sanofi-Aventis, Novo Nordisk, Novartis, AstraZeneca, Sanwakagaku, Ono, MSD, Boehringer Ingelheim, Kissei, Takeda, Daiichi Sankyo, and Eli Lilly.
Submitted: March 18, 2013; **Accepted:** May 29, 2014.
Reference information: *J Clin Invest*. 2014;124(8):3634–3644. doi:10.1172/JCI69866.

Autophagy is a cellular protein degradation system and plays a crucial role in intracellular quality control by eliminating damaged organelles and toxic proteins (20–22). It has been reported that intracellular accumulation of abnormal proteins in neurodegenerative diseases, such as amyloid plaque formation in Alzheimer's disease, is associated with malfunction of autophagy (23–25). Under increased insulin resistance in obese subjects, autophagy is activated within β cells, which leads to increased capacity for insulin secretion through replication of β cells and inhibition of apoptosis (26). We reported previously the accumulation of ubiquitinated proteins, damaged mitochondria, and marked deterioration in glucose tolerance in pancreatic β cell–specific *Atg7*-deficient mice (*Atg7$^{fl/fl}$:RIP-Cre*) (26, 27). Thus, autophagy functions as a cell-protective mechanism. Autophagy is upregulated when cells are preparing to rid themselves of damaging cytoplasmic components, such as damaged organelles, aggregate-prone proteins, or disease-related toxic oligomers (20–22).

In the present study, we showed that hIAPP not only induced apoptosis, but also suppressed growth factor–induced proliferation of INS-1 cells. Furthermore, expression of hIAPP stimulated autophagosome formation, and microRNA-mediated knockdown of *Atg7* sensitized INS-1 cells to hIAPP-induced cytotoxicity. Genetic analysis was subsequently conducted to determine the role of autophagy in hIAPP cytotoxicity and the functional interaction between hIAPP and the autophagy machinery in vivo.

Results

hIAPP treatment induces autophagy in pancreatic β cells. To examine the toxic effect of hIAPP on β cells and its relation to autophagy, INS-1 cells were treated with hIAPP. Consistent with previous reports (28), treatment of INS-1 cells with hIAPP, but not rat IAPP (rIAPP), induced dose-dependent reduction in the viability of INS-1 cells (Supplemental Figure 1A; supplemental material available online with this article; doi:10.1172/JCI69866DS1). Several studies have demonstrated that hIAPP induces β cell apoptosis (8, 9, 29, 30). Consistent with these reports, hIAPP-induced apoptosis of INS-1 cells was confirmed by cleaved caspase-3 activation (Supplemental Figure 1B). Furthermore, cell viability was reduced, and cell apoptosis enhanced, by exogenous hIAPP expression by adenovirus compared with rIAPP (Supplemental Figure 2). Thus, hIAPP peptide and hIAPP expressed by adenovirus elicit a proper biological response in INS-1 cells.

Morita et al. previously reported that the formation of autophagosomes and the conversion of microtubule-associated protein light chain 3B–I (LC3B-I) to LC3B-II was enhanced in hIAPP-expressing COS-1 cells (31). To evaluate the steady-state level of autophagy during treatment with hIAPP, electron microscopic analysis was performed in INS-1 cells in the presence of 2 μM hIAPP or rIAPP peptide for 12 hours. Compared with rIAPP, the expression of hIAPP increased the number of autophagic vacuoles, which were recognized as double-membrane structures containing visible cytoplasmic content (Figure 1, A and B). To assess whether the increased number of autophagosomes at steady state was due to increased autophagy flux or blockade of autophagy cascade after the formation of autophagosomes, immunoblot and immunofluorescence analyses were performed. Treatment of INS-1 cells with hIAPP increased LC3-II levels, while the protein level of p62 (also known as SQSTM1), a specific substrate for autophagy (32–34), was not affected (Figure 1C and Supplemental Figure 3), which suggests that increased LC3-II levels were probably due to increased autophagic activity. Furthermore, the addition of lysosome inhibitor to hIAPP-treated INS-1 cells increased LC3-II levels, providing further support for the role of hIAPP in the activation of autophagy flux. Consistent with these results, transduction of INS-1 cells with hIAPP-expressing adenovirus, but not rIAPP, also increased LC3-II levels, although p62 protein levels were not changed (Supplemental Figure 4). These in vitro findings were also verified in vivo using hIAPP-knockin mice (referred to herein as *hIAPP:Atg7$^{fl/fl}$* mice; see Methods). We reported previously that high-fat diet feeding upregulated autophagic vacuole formation in pancreatic β cells in response to increased insulin resistance (26). Thus, EM analysis was next performed to examine the formation of autophagosomes in β cells of *hIAPP:Atg7$^{fl/fl}$* and *Atg7$^{fl/fl}$* mice (Figure 1, D–G). Morphometric analysis showed a significantly higher number of autophagosomes in β cells of *hIAPP:Atg7$^{fl/fl}$* versus *Atg7$^{fl/fl}$* mice (Figure 1H). Furthermore, immunoblot analysis showed that p62 did not accumulate in islets of *hIAPP:Atg7$^{fl/fl}$* mice (Supplemental Figure 5). These results indicate that hIAPP expression accelerates autophagy formation under high-fat diet–induced insulin resistance.

Effects of hIAPP/rIAPP and autophagy deficiency on cell cycle and viability of INS-1 cells. To examine the effect of reduced autophagic activity on β cells, we used INS-1 cells in which *Atg7* was inducibly knocked down (referred to herein as Atg7-KD INS-1 cells) based on the expression of microRNAs (35). Treatment with tetracycline for 3 days resulted in significant suppression of ATG7 expression and concomitant accumulation of p62, a specific substrate of autophagic degradation (Figure 2A and refs. 33, 34). Knockdown of *Atg7* in the presence of hIAPP, but not rIAPP, had an additive toxic effect on cell viability (Figure 2B), which suggests that reduced autophagic activity sensitized β cells to the cytotoxic effects of hIAPP. These additive toxic effects were also observed in Atg7-KD INS-1 cells infected with adenovirus expressing hIAPP rather than rIAPP (Supplemental Figure 6).

Given that cell number is regulated by a balance between cell death and cell proliferation, we explored the effects of hIAPP on the proliferation of INS-1 cells. The cells were growth arrested with 2.8 mM glucose and 0.5% FCS for 24 hours, then released with 22.2 mM glucose, 0.5% FCS, and 200 nM insulin in the presence or absence of IAPP for 24 hours. Unlike INS-1 cells treated with rIAPP, where nearly 50% were actively engaged in the cell cycle (S and G2/M), INS-1 cells treated with 8 μM hIAPP showed a high proportion engaged in G0/G1 and 17% in S and G2/M (Figure 2, C and D). This suppression of cell cycle progression by hIAPP was consistent with the low number of INS-1 cells after treatment with hIAPP (Figure 2B). Knockdown of *Atg7* resulted in similar inhibition of cell cycle progression of INS-1 cells, but no further additive effect was observed by treatment with hIAPP (Figure 2D).

Physiological parameters in hIAPP-knockin and β cell–specific Atg7 knockout mice. Our results suggested that autophagy plays a protective role in β cells against hIAPP-induced cell toxicity (Figure 2B and Supplemental Figure 6). Next, to assess the pathophysiological role of hIAPP in vivo and its potential link to autophagy, we generated hIAPP-knockin mice with β cell–specific deletion of *Atg7* (see Methods). The use of standard diet up to 20 weeks of age

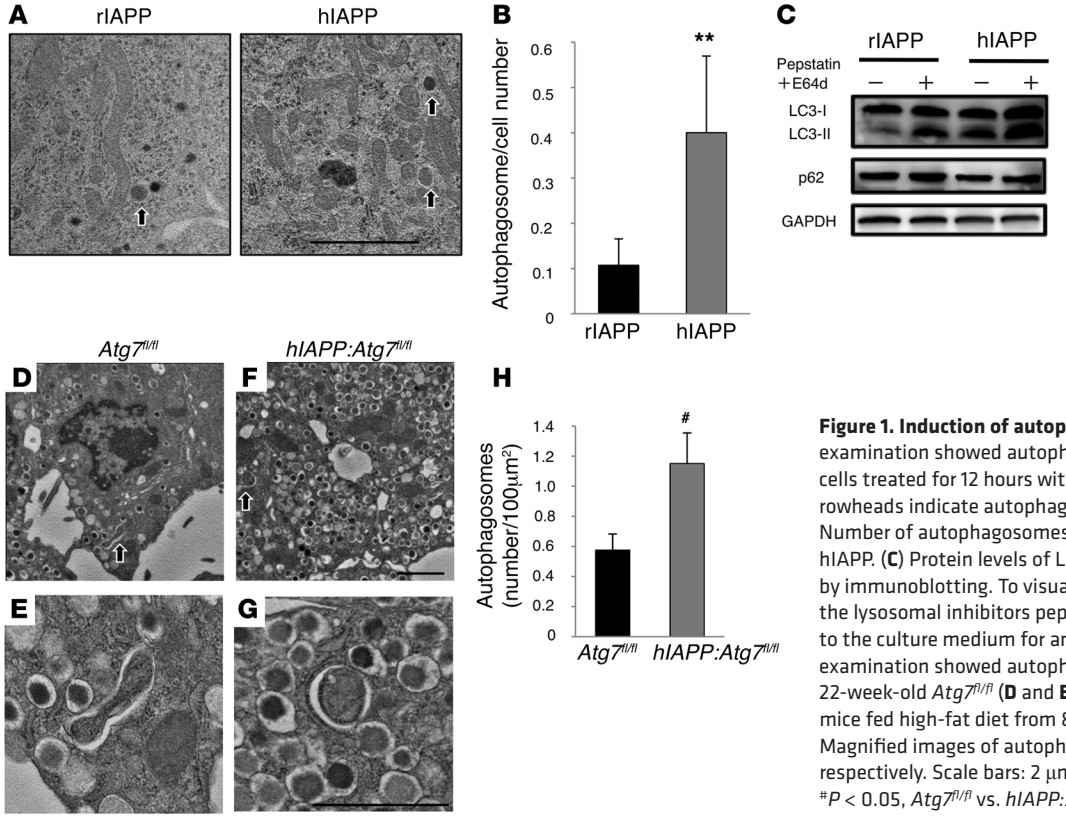

Figure 1. Induction of autophagy by hIAPP. (**A**) EM examination showed autophagosome formation in INS-1 cells treated for 12 hours with rIAPP or hIAPP peptide. Arrowheads indicate autophagosomes. Scale bar: 2 μm. (**B**) Number of autophagosomes per cell. $^{**}P < 0.01$, rIAPP vs. hIAPP. (**C**) Protein levels of LC3, p62, and GAPDH, assessed by immunoblotting. To visualize accumulation of LC3-II, the lysosomal inhibitors pepstatin A and E64d were added to the culture medium for an additional 6 hours. (**D**–**G**) EM examination showed autophagosome formation in β cells of 22-week-old *Atg7*$^{fl/fl}$ (**D** and **E**) and *hIAPP:Atg7*$^{fl/fl}$ (**F** and **G**) mice fed high-fat diet from 8 to 20 weeks of age. (**E** and **G**) Magnified images of autophagosomes (arrows) in **D** and **F**, respectively. Scale bars: 2 μm. (**H**) Autophagosome counts. $^{\#}P < 0.05$, *Atg7*$^{fl/fl}$ vs. *hIAPP:Atg7*$^{fl/fl}$.

resulted in progressive and comparable weight gain in *Atg7*$^{fl/fl}$ and *Atg7*$^{fl/fl}$*:Cre* mice (Figure 3A). However, *Atg7*$^{fl/fl}$*:Cre* mice gained more weight than *Atg7*$^{fl/fl}$ animals with high-fat diet feeding (Figure 3E). *RIP-Cre* can induce ectopic Cre expression in a subset of cells that interact with hypothalamic proopiomelanocortin-positive (POMC-positive) neurons (36). Recently, POMC neuron–specific deletion of *Atg7* was shown to result in body weight gain (37). Taken together, these results suggest that the body weight gain was probably due to loss of autophagy in hypothalamic neurons. hIAPP-knockin mice gained more weight than those with endogenous murine *Iapp*, under both standard diet and high-fat diet (Figure 3, A and E). This difference in body weight gain most likely reflects differences in food intake, which was significantly larger in hIAPP-knockin mice than in mice with endogenous murine *Iapp* (Figure 3, B and F).

Impaired glucose tolerance in hIAPP-knockin mice with autophagy dysfunction. While there was no difference in nonfasting blood glucose level between *hIAPP:Atg7*$^{fl/fl}$ and *Atg7*$^{fl/fl}$ mice fed standard diet, a modest but significant rise in nonfasting blood glucose level was observed in *hIAPP:Atg7*$^{fl/fl}$ versus *Atg7*$^{fl/fl}$ mice fed high-fat diet (Figure 3, C and G). On the other hand, at 8 and 20 weeks of age, glucose tolerance was comparable between *hIAPP:Atg7*$^{fl/fl}$ and *Atg7*$^{fl/fl}$ mice fed standard diet and high-fat diet (Figure 3, D and H, and Supplemental Figure 7). Given the discrepancy between nonfasting blood glucose level and glucose tolerance (Figure 3, G and H), whether hIAPP caused deterioration of glucose tolerance independent of its effect on body weight remains inconclusive, because there was a significant increase in body weight in high-fat diet–fed *hIAPP:Atg7*$^{fl/fl}$ versus *Atg7*$^{fl/fl}$ mice (Figure 3E). To exclude the effects of differences in body weight, average body weight of all groups was adjusted to approximately 45 g, by choosing 9–11 mice ranging 40–50 g per group analyzed in Figure 3 (Figure 4A). In this weight-matched comparison, there was no significant difference between high-fat diet–fed *hIAPP:Atg7*$^{fl/fl}$ and *Atg7*$^{fl/fl}$ mice in either nonfasting blood glucose level or glucose tolerance (Figure 4, B and C). These results indicate that hIAPP does not cause deterioration of glucose tolerance, even in the presence of insulin resistance. Consistent with our previous study (26), deletion of *Atg7* in pancreatic β cells resulted in significantly higher nonfasting blood glucose level compared with *Atg7*-intact controls under both standard and high-fat diet (Figure 3, C and G). As reported previously by our group (26), *Atg7*-deficient mice showed significant impairment of glucose tolerance under standard diet (Figure 3D). No deterioration of glucose tolerance was observed in standard diet–fed *hIAPP:Atg7*$^{fl/fl}$*:Cre* versus *Atg7*$^{fl/fl}$*:Cre* mice, whereas significant deterioration of glucose tolerance was observed in high-fat diet–fed *hIAPP:Atg7*$^{fl/fl}$*:Cre* versus *Atg7*$^{fl/fl}$*:Cre* mice (Figure 3, D and H). The same tendency was also observed after adjustment for body weight (Figure 4C). These results suggest potentiation of hIAPP cytotoxicity in autophagy-impaired β cells in the presence of insulin resistance. To gain mechanistic insight into the deterioration of glucose tolerance observed in high-fat diet–fed *hIAPP:Atg7*$^{fl/fl}$*:Cre* versus *Atg7*$^{fl/fl}$*:Cre* mice (Figure 3H), insulin secretion and insulin sensitivity were assessed. The results showed no difference in plasma insulin level during intraperitoneal glucose tolerance test (IPGTT) or in blood glucose curve during insulin tolerance test (ITT) between *Atg7*$^{fl/fl}$*:Cre* and *hIAPP:Atg7*$^{fl/fl}$*:Cre* mice (Supplemental Figures 8 and 9). However, glucose-stimulated insulin secretion from *hIAPP:Atg7*$^{fl/fl}$*:Cre* islets was reduced compared with *Atg7*$^{fl/fl}$*:Cre* islets (Supplemental Figure 10). These results can

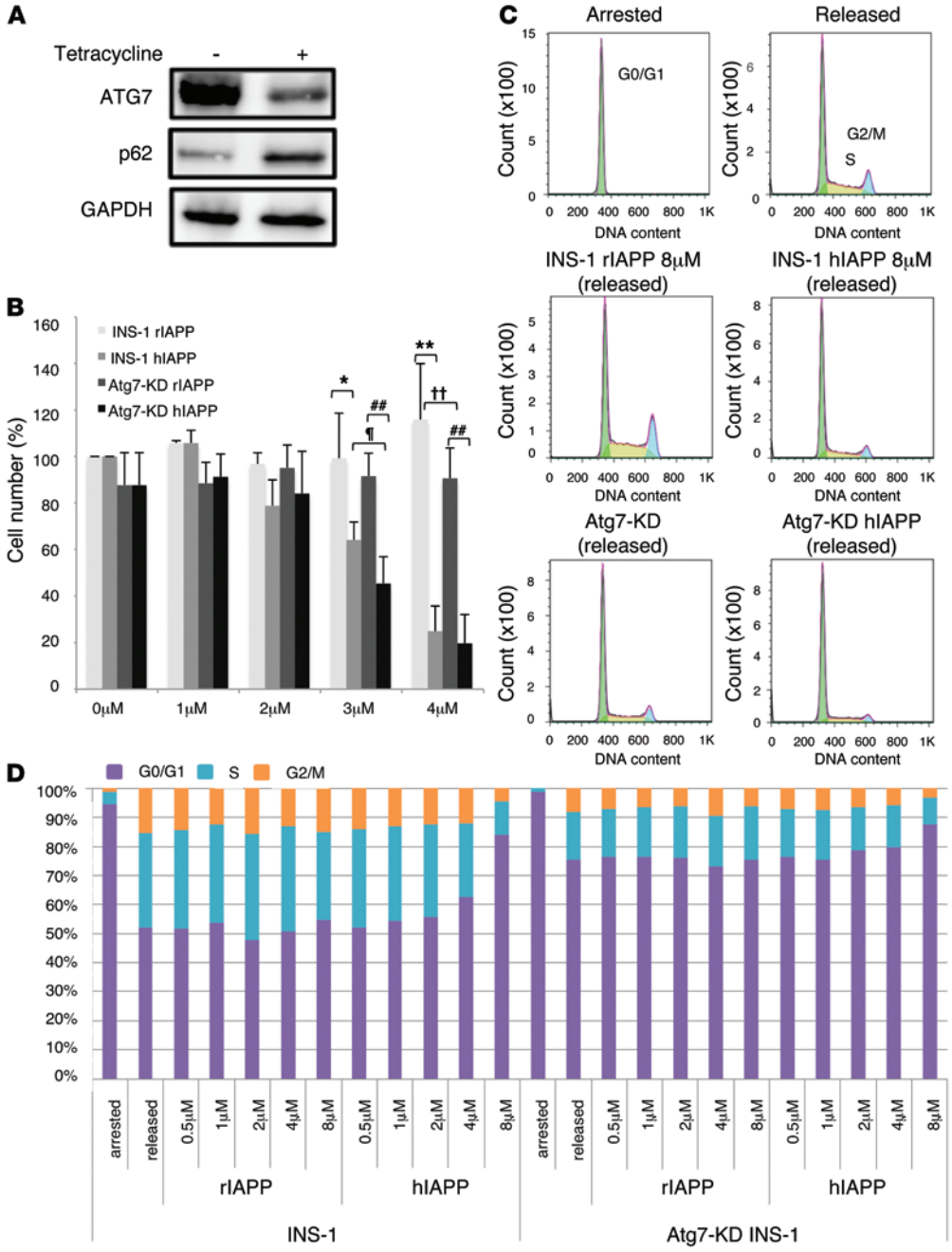

Figure 2. Effects of hIAPP/rIAPP and autophagy deficiency on cell cycle and viability of INS-1 cells. (**A**) Association of reduced ATG7 with accumulation of p62 in Atg7-KD INS-1 cells with tetracycline supplementation. GAPDH served as loading control. (**B**) INS-1 and Atg7-KD INS-1 cells were cultured in the presence of 0–4 μM rIAPP or hIAPP peptide for 48 hours. The number of cells not stained with Trypan Blue was counted; cell number is presented as percentage of control (0 μM IAPP). $^{*}P < 0.05$, $^{**}P < 0.01$, INS-1 rIAPP vs. INS-1 hIAPP; $^{\dagger\dagger}P < 0.01$, INS-1 rIAPP vs. Atg7-KD rIAPP; $^{\#\#}P < 0.01$, Atg7-KD rIAPP vs. Atg7-KD hIAPP; $^{\P}P < 0.05$, INS-1 hIAPP vs. Atg7-KD hIAPP. (**C** and **D**) FACS histograms (**C**) and stacked bar graphs (**D**) of INS-1 cells grown under conditions of growth arrest (induced by exposure to 2.8 mMol/l glucose and serum withdrawal for >24 hours) and after release from arrest (by 22.2 mMol/l glucose, 200 nMol/l insulin, hIAPP/rIAPP, and serum withdrawal medium for 24 hours).

probably explain the deterioration of glucose tolerance in hIAPP-knockin mice with autophagy dysfunction.

β cell mass, replication, and apoptosis in Atg7-deficient hIAPP-knockin mice. To gain mechanistic insight into the failure of *Atg7*-deficient hIAPP-knock-in mice in preserving normal glucose tolerance in response to metabolic demands, we assessed β cell mass. When mice were fed standard diet, autophagy deficiency (*Atg7$^{fl/fl}$:Cre*) or replacement of endogenous *Iapp* with *hIAPP* (*hIAPP:Atg7$^{fl/fl}$*) had minimal effects on β cell mass compared with the control (*Atg7$^{fl/fl}$*) (Figure 5A). On the other hand, while 12-week high-fat diet feeding resulted in a 3.1-fold increase in β cell mass in *Atg7$^{fl/fl}$* mice, less significant increases were observed in *hIAPP:Atg7$^{fl/fl}$* and *Atg7$^{fl/fl}$:Cre* mice (1.7- and 2.2-fold, respectively; Figure 5A). Taken together, these results suggest that hIAPP knockin or deficiency of autophagy inhibit the high-fat diet–induced compensatory increase in β cell mass observed. Importantly, no compensatory increase in β cell mass was observed in *hIAPP:Atg7$^{fl/fl}$:Cre* mice (1.1-fold; Figure 5A), which indicates that hIAPP and autophagy deficiency inhibit in additive or synergistic fashion the compensatory increase in β cell mass in vivo, in agreement with our in vitro results (Figure 2B and Supplemental Figure 6). As reported previously (26), the increase in the number of cleaved caspase-3–positive cells in *Atg7$^{fl/fl}$:Cre* islets confirmed increased apoptosis, which was responsible for the failure of the high-fat diet–induced compensatory increase in β cell mass in the presence of autophagy deficiency (Figure 5B). Similarly, an increase in the number of cleaved caspase-3–positive apoptotic cells was observed in *hIAPP:Atg7$^{fl/fl}$* islets. 12-week high-fat diet feeding stimulated significant β cell replication in *Atg7$^{fl/fl}$* islets, as assessed by the percentage of Ki-67–positive cells (2.8%; Figure 5C and ref. 38). In contrast, the number of Ki-67–positive cells was significantly lower in *hIAPP:Atg7$^{fl/fl}$* than *Atg7$^{fl/fl}$* islets (Figure 5C). Collectively, these results suggest that reduction in β cell replication, as well as induction of β cell apoptosis, may account for the failure of compensatory increase in β cell mass caused by hIAPP. Similarly, as described previously (26), the low number of Ki-67–positive cells in *Atg7$^{fl/fl}$:Cre*

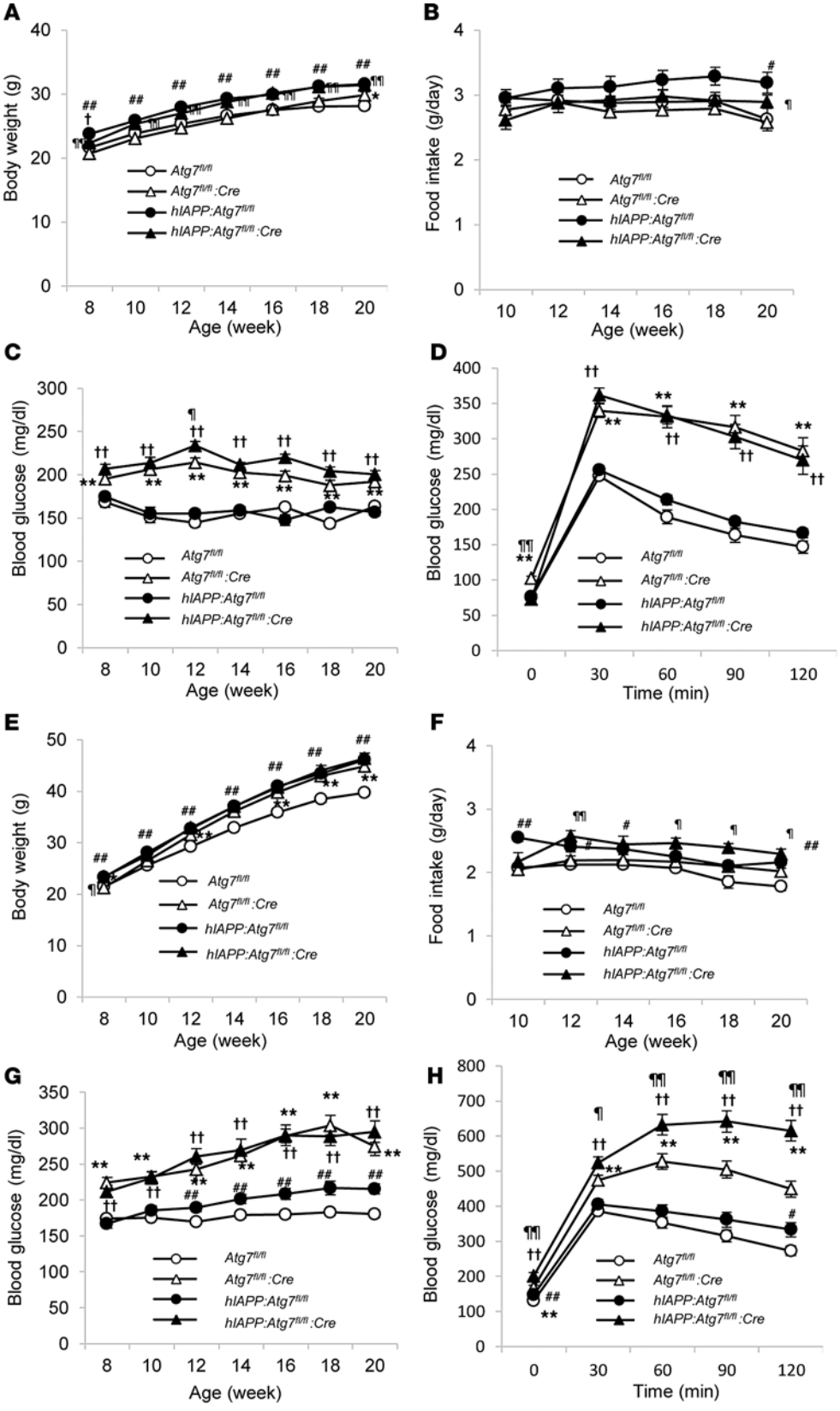

Figure 3. Physiological parameters. Mice were fed standard diet (**A**–**D**) or high-fat diet (**E**–**H**) from 8 to 20 weeks of age. Shown are body weight (**A** and **E**), food intake (**B** and **F**), nonfasting blood glucose levels (**C** and **G**), and glucose tolerance (**D** and **H**) of *Atg7$^{fl/fl}$* (n = 31 [standard], 49 [high-fat]), *Atg7$^{fl/fl}$:Cre* (n = 38 [standard], 39 [high-fat]), *hIAPP:Atg7$^{fl/fl}$* (n = 31 [standard], 32 [high-fat]), and *hIAPP:Atg7$^{fl/fl}$:Cre* (n = 19 [standard], 27 [high-fat]) mice. Data are mean ± SEM. $^{*}P < 0.05$, $^{**}P < 0.01$, *Atg7$^{fl/fl}$* vs. *Atg7$^{fl/fl}$:Cre*; $^{\dagger}P < 0.05$, $^{\dagger\dagger}P < 0.01$, *hIAPP:Atg7$^{fl/fl}$* vs. *hIAPP:Atg7$^{fl/fl}$:Cre*; $^{\#}P < 0.05$, $^{\#\#}P < 0.01$, *Atg7$^{fl/fl}$* vs. *hIAPP:Atg7$^{fl/fl}$*; $^{\P}P < 0.05$, $^{\P\P}P < 0.01$, *Atg7$^{fl/fl}$:Cre* vs. *hIAPP:Atg7$^{fl/fl}$:Cre*.

islets (Figure 5C) confirmed the critical role of β cell autophagy in retaining high-fat diet–induced β cell proliferation.

Histopathological findings in islets of Atg7-deficient hIAPP-knockin mice. Next, we evaluated whether the changes in β cell function were associated with changes in islet morphology. H&E staining of islets of 20-week-old high-fat diet–fed *Atg7$^{fl/fl}$:Cre* mice showed degenerative changes (Figure 6, A and C), as described previously (26). Despite the presence of highly degenerated β cells (described as ''balloon-like''), many morphologically normal-looking insulin-positive cells were also found in the *Atg7$^{fl/fl}$:Cre* islets (Figure 6G). In agreement with the low β cell mass described above (Figure 5A), degeneration of islets was more pronounced upon replacement of endogenous murine *Iapp* with *hIAPP*; the number of insulin-positive cells was reduced (Figure 6, E–H).

Autophagy is responsible for constitutive protein turnover in various cell types, and defective autophagy is associated with accumulation of large, ubiquitin-containing inclusion bodies with overexpression of LC3-binding protein p62 (33, 39). We reported previously the presence of p62-containing inclusion bodies and accelerated formation of these inclusions after high-fat diet feeding in *Atg7*-deficient degenerating β cells (26). In contrast to the large p62-positive inclusions we observed in *Atg7$^{fl/fl}$:Cre* islets, surprisingly, these inclusions were almost completely dispersed throughout the cytoplasm in *hIAPP:Atg7$^{fl/fl}$:Cre* islet cells (Figure 7, A–D). This finding suggests that hIAPP disrupts inclusion formation, and the cytoplas-

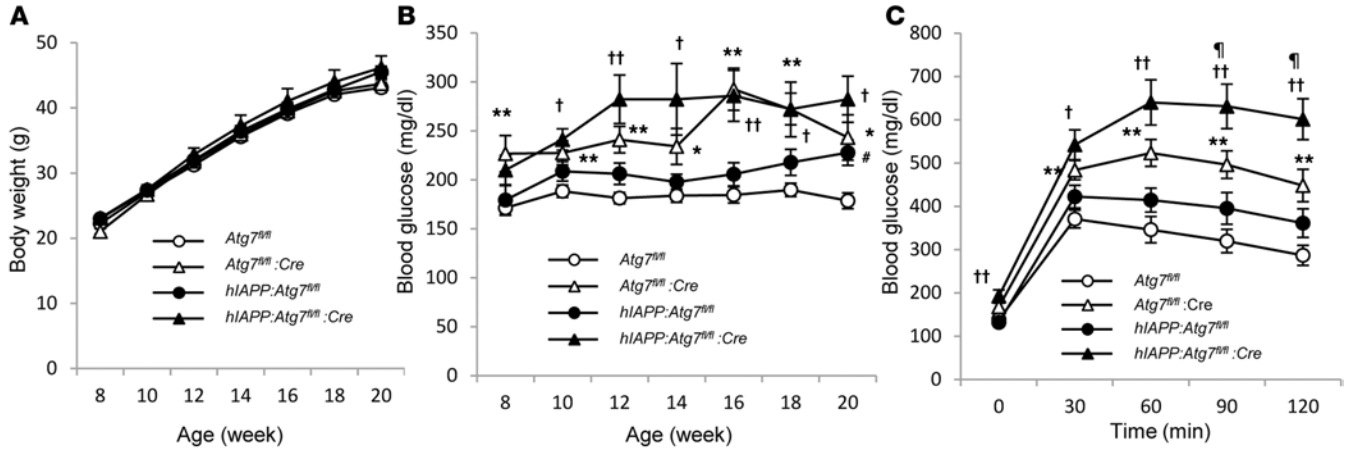

Figure 4. Physiological parameters after adjustment for body weight. *Atg7*$^{fl/fl}$ (n = 9), *Atg7*$^{fl/fl}$*:Cre* (n = 11), *hIAPP:Atg7*$^{fl/fl}$ (n = 10), and *hIAPP:Atg7*$^{fl/fl}$*:Cre* (n = 11) mice were fed high-fat diet from 8 to 20 weeks of age as in Figure 3, E–H. Adjusted values for (**A**) body weight, (**B**) nonfasting blood glucose, and (**C**) glucose tolerance correspond to results in Figure 3, E, G, and H, respectively. Data are mean ± SEM. $^{**}P < 0.01$, *Atg7*$^{fl/fl}$ vs. *Atg7*$^{fl/fl}$*:Cre*; $^{\dagger}P < 0.05$, $^{\dagger\dagger}P < 0.01$, *hIAPP:Atg7*$^{fl/fl}$ vs. *hIAPP:Atg7*$^{fl/fl}$*:Cre*; $^{\#}P < 0.05$, *Atg7*$^{fl/fl}$ vs. *hIAPP:Atg7*$^{fl/fl}$; $^{\P}P < 0.05$, *Atg7*$^{fl/fl}$*:Cre* vs. *hIAPP:Atg7*$^{fl/fl}$*:Cre*.

mic redistribution of p62-positive aggregates may be indicative of a causal relationship between the presence of hIAPP and the phenotype exacerbation in *hIAPP:Atg7*$^{fl/fl}$*:Cre* mice.

It has been proposed that soluble toxic oligomers for hIAPP, rather than insoluble hIAPP amyloid fibrils, are responsible for hIAPP-induced cytotoxicity (9, 40). To explore such a scenario, we investigated the presence of toxic oligomers in hIAPP-knockin islets using A11 antibody, which recognizes a backbone peptide epitope common to amyloid oligomers (41, 42). Interestingly, intense A11 signals, almost completely colocalized with those for p62, were detected (Figure 7, E–H), which suggests the abundant presence of some unknown toxic oligomers in *Atg7*-deficient β cells and their close association with the adaptor protein p62. Taken together, these results suggest that hIAPP maintains the solubility and toxicity of p62-associated oligomers by preventing the formation of insoluble cytoplasmic inclusions (32–34).

Our final set of experiments tested whether reduced autophagic activity in β cells permits hIAPP amyloid fibril formation. For this purpose, autophagy-deficient hIAPP-knockin mice were examined for the presence of amyloid plaques. Extensive histological analysis using congo-red staining, direct fast scarlet staining, and thioflavin-S staining showed no amyloid formation in *hIAPP:Atg7*$^{fl/fl}$*:Cre* mice fed high-fat diet to at least 22 weeks of age. In contrast, amyloid was readily detected in the islet specimen of human T2DM (Supplemental Figure 11).

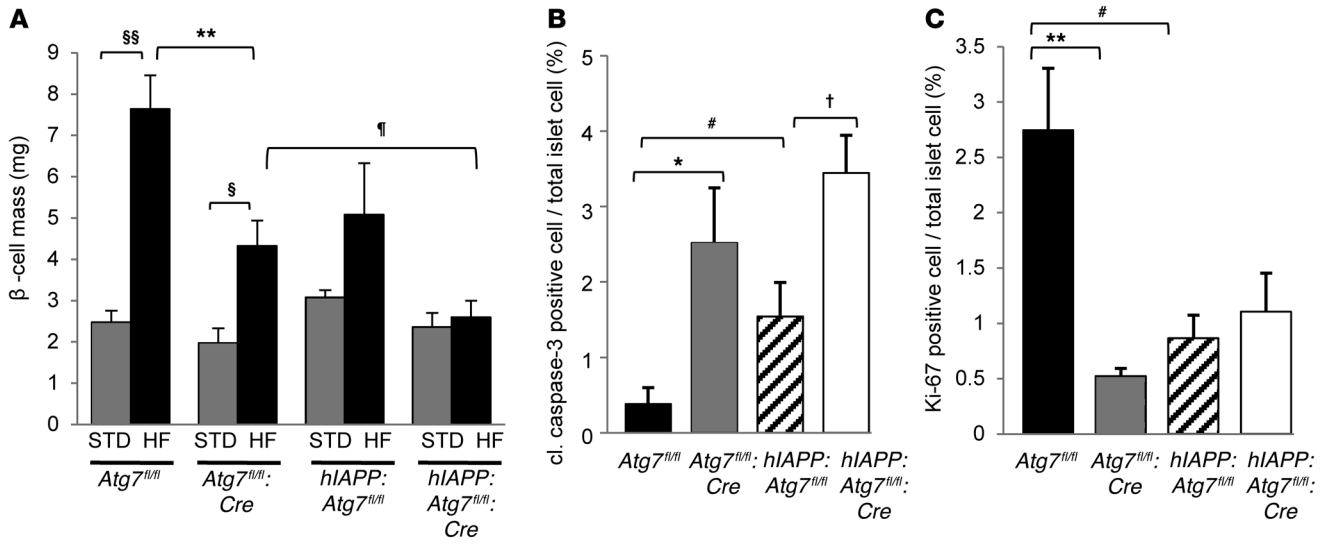

Figure 5. Effect of hIAPP knockin and autophagy deficiency on β cell mass. (**A**) β cell mass of *Atg7*$^{fl/fl}$, *Atg7*$^{fl/fl}$*:Cre*, *hIAPP:Atg7*$^{fl/fl}$, and *hIAPP:Atg7*$^{fl/fl}$*:Cre* mice fed standard (STD) or high-fat (HF) diet. (**B** and **C**) Number of cleaved caspase-3–positive (**B**) and Ki-67–positive (**C**) intraislet cells in high-fat diet–fed mice of each genotype. In **A**–**C**, 5 mice per genotype were prepared for morphometric analysis. Data are mean ± SEM. $^{\S}P < 0.05$, $^{\S\S}P < 0.01$, standard vs. high-fat; $^{*}P < 0.05$, $^{**}P < 0.01$, *Atg7*$^{fl/fl}$ vs. *Atg7*$^{fl/fl}$*:Cre*; $^{\dagger}P < 0.05$, *hIAPP:Atg7*$^{fl/fl}$ vs. *hIAPP:Atg7*$^{fl/fl}$*:Cre*; $^{\#}P < 0.05$, *Atg7*$^{fl/fl}$ vs. *hIAPP:Atg7*$^{fl/fl}$; $^{\P}P < 0.05$, *Atg7*$^{fl/fl}$*:Cre* vs. *hIAPP:Atg7*$^{fl/fl}$*:Cre*.

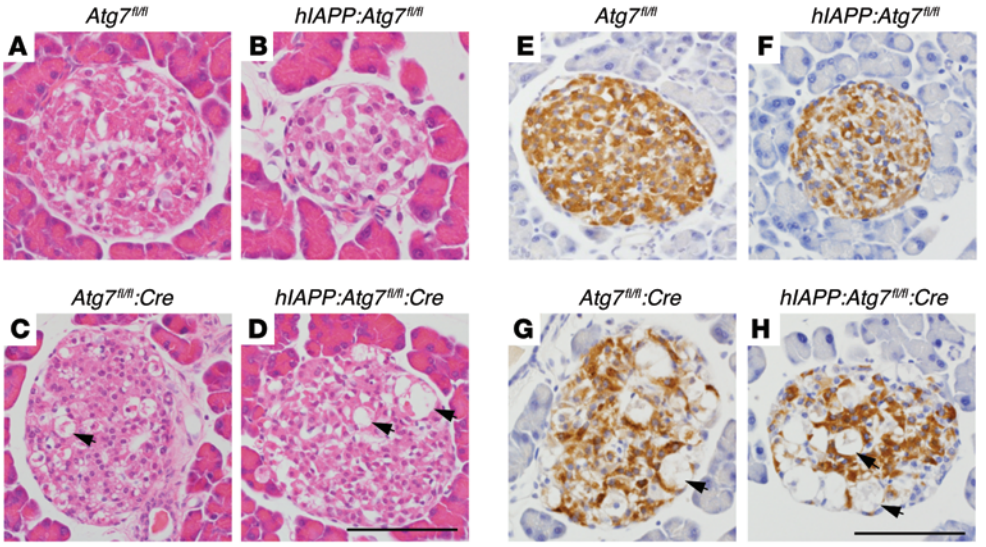

Figure 6. Islet morphology. Shown is the morphology of representative islets from *Atg7*$^{fl/fl}$ (**A** and **E**), *hIAPP:Atg7*$^{fl/fl}$ (**B** and **F**), *hIAPP:Atg7*$^{fl/fl}$ (**C** and **G**), and *hIAPP:Atg7*$^{fl/fl}$*:Cre* (**D** and **H**) mice fed high-fat diet from 8 to 20 weeks of age. Arrowheads indicate degenerative "balloon-like" β cells. (**A**–**D**) H&E staining. (**E**–**H**) Insulin staining. Scale bars: 50 μm.

Discussion

The hIAPP-knockin mouse model used in the present study allowed for assessment of the role of hIAPP in a physiological setting. In contrast to the previously described transgenic models for hIAPP (13–15), hIAPP-knockin mice remained healthy and showed normal glucose tolerance as long as they were fed standard diet. However, hIAPP cytotoxicity became evident with high-fat diet feeding, and loss of autophagy and such effects were observed even after adjustment for body weight among the 4 groups (Figure 4). Our observations suggested that hIAPP is not intrinsically cytotoxic, but behaves as a susceptibility factor for human T2DM together with other risk factors for diabetes, such as insulin resistance, high-fat feeding, and/or reduced autophagy (26, 27). In contrast, overexpression of hIAPP in vitro or in vivo by a transgenic approach uncovered a broad range of toxic properties for hIAPP on β cells, including induction of apoptosis (5, 14, 43), amyloidogenesis (14, 15, 44), mitochondrial dysfunction (45), and inhibition of GSIS (46), possibly due to a nonselective toxic effect of hIAPP as an inducer of membrane disruption at pharmacological concentrations (9, 45, 47). In contrast, in the present study, the phenotype derived from endogenous hIAPP turned out to be limited, modest, and specific. Our studies circumvent a main caveat of transgenic studies, which may not recapitulate the function of hIAPP in a physiological context. Thus, the hIAPP-knockin mouse is a potentially useful humanized mouse model for further in vivo characterization of hIAPP-associated pathology of T2DM.

On the other hand, our study design imposed certain limitations. *Atg7* deletion in extrapancreatic tissues might have caused the obese phenotype. Due to misexpression of *RIP-Cre* in the hypothalamus (48), RIP-mediated *Atg7* deletion might have caused increased food intake and obesity with high-fat diet feeding (36, 37). In addition, replacement of endogenous murine *Iapp* with *hIAPP* by the hIAPP-knockin strategy induced increased food consumption and body weight gain (Figure 3). While mouse IAPP intrinsically functions as a satiety factor acting on the CNS, such function is probably less active with hIAPP, based on its aggregation-prone properties (49). Nevertheless, we provided evidence of the cell-autonomous harmful effects of hIAPP on β cell function. Indeed, compared with C57BL/6J control islets, those of *hIAPP*-homozygous mice were less capable of normalizing glucose homeostasis when transplanted into diabetic mice (A. Hara and Y. Fujitani, unpublished observations). Thus, the metabolic phenotype caused by hIAPP knockin and *Atg7* disruption appears to be derived both from a direct effect on pancreatic β cell function and from an indirect effect on the CNS.

Previous studies reported that exogenously expressed hIAPP in COS-1 cells (31) or transgenically overexpressed hIAPP in mouse β cells (50) was cytotoxic. Expression of hIAPP in COS-1 cells (31) or in β cells (50) increased autophagosome formation, with increased conversion of LC3-I to LC3-II. Morita et al. previously reported that chemical suppression of autophagy by 3-MA resulted in acceleration of hIAPP-induced apoptosis, whereas enhancement of autophagy by rapamycin caused inhibition of apoptosis (31). Furthermore, inactivation of autophagy by siRNA against *Atg5* caused further decrement in cell viability. Based on these results, the authors proposed that autophagy seems to play a beneficial role by protecting β cells against hIAPP-induced apoptosis, although their study was mainly carried out using COS-1 cells (31). Consistent with these results, we found that hIAPP was cytotoxic in native β cells and INS-1 cells. Our present observations (Figures 2–5) further strengthened the conclusion that hIAPP-induced toxicity is negatively regulated by autophagy. Interestingly, Rivera et al. reported recently that transgenic overexpression of hIAPP disrupted the autophagy/lysosomal pathway in pancreatic β cells (50). In rats transgenic for hIAPP (HIP rats), cytoplasmic inclusions positive for p62 were detected, presumably due to the suppression of autophagic degradation by hIAPP (50). Conversely, in this study, *hIAPP:Atg7*$^{fl/fl}$ mice showed no evidence of impaired autophagy in β cells: in contrast to the effects of hIAPP in HIP rats, no intracellular aggregates positive for p62 were observed in *hIAPP:Atg7*$^{fl/fl}$ islets, and p62 did not accumulate in islets expressing physiological levels of hIAPP in vivo (Figure 7F and Supplemental Figure 5). Thus, expression of *hIAPP* from the endogenous murine *Iapp* locus presumably does not reach the threshold level at which hIAPP can induce autophagic dysfunction.

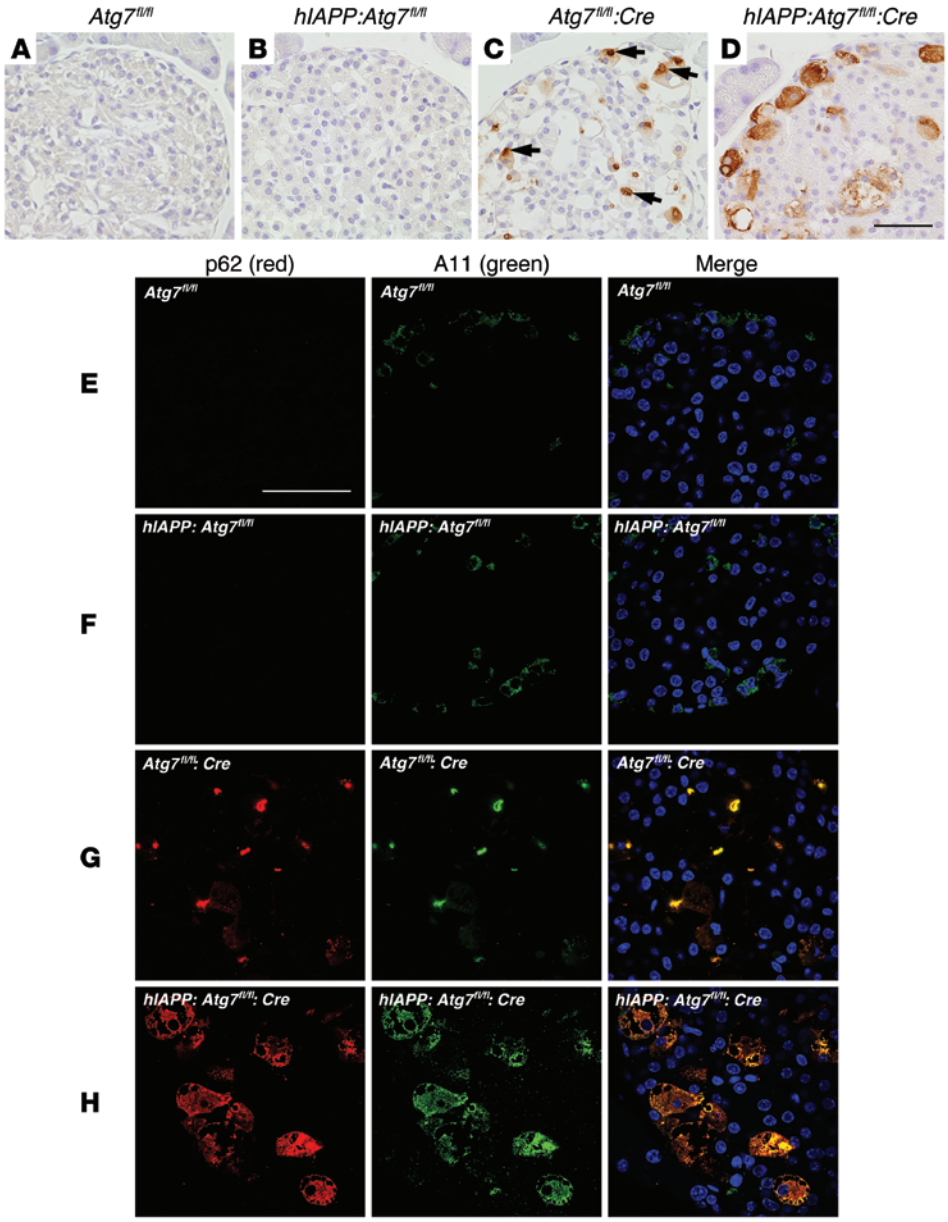

Figure 7. hIAPP inhibits formation of cytoplasmic inclusions immunopositive for p62 in *Atg7$^{fl/fl}$:Cre* islets. (**A**–**D**) Representative section of the pancreas of 22-week-old high-fat diet–fed *Atg7$^{fl/fl}$* (**A**), *hIAPP:Atg7$^{fl/fl}$* (**B**), *Atg7$^{fl/fl}$:Cre* (**C**), and *hIAPP:Atg7$^{fl/fl}$:Cre* (**D**) mice, immunohistochemically stained for p62. The p62-positive signal accumulated as inclusions (arrows) within islet cells of *Atg7$^{fl/fl}$:Cre* mice, but were dispersed throughout the cytoplasm in *hIAPP:Atg7$^{fl/fl}$:Cre* mice. Scale bar: 200 μm. (**E**–**H**) Confocal images of pancreas sections from 22-week-old high-fat diet–fed *Atg7$^{fl/fl}$* (**E**), *hIAPP:Atg7$^{fl/fl}$* (**F**), *Atg7$^{fl/fl}$:Cre* (**G**), and *hIAPP:Atg7$^{fl/fl}$:Cre* (**H**) mice stained for p62, A11, and cell nuclei (blue). Staining of toxic oligomer was intense in *Atg7$^{fl/fl}$:Cre* and *hIAPP:Atg7$^{fl/fl}$:Cre* islets, but faint in *Atg7$^{fl/fl}$* and *hIAPP:Atg7$^{fl/fl}$* islets. p62 was largely colocalized with A11-positive staining in *Atg7$^{fl/fl}$:Cre* and *hIAPP:Atg7$^{fl/fl}$:Cre* islets. Scale bar: 50 μm.

In addition to the induction of apoptosis, we found that hIAPP inhibited high glucose- and insulin-induced cell cycle progression of β cells (Figure 2), which has been overlooked to date. This unappreciated role of hIAPP was further verified in vivo in hIAPP-knockin mice (Figure 5). This finding may explain, at least in part, the failure of correct expansion of β cell mass in humans under an insulin resistance state. Future studies should focus on the molecular mechanisms of hIAPP-mediated inhibition of β cell proliferation induced by growth factors or peripheral insulin resistance. Furthermore, studies that examine the physiological regulation of human β cell proliferation should provide therapeutic cues in the future and preparation of large number of human β cells for cell-based therapies directed against type 1 and type 2 diabetes.

Amyloid deposition is the hallmark of human diabetic islets (7, 8). Thus, we examined our mutant mice for amyloid deposition. The results showed lack of amyloid deposits even in 34-week-old high-fat diet–fed *hIAPP:Atg7$^{fl/fl}$:Cre* mice. To date, various transgenic rodent models for hIAPP have been reported; some showed amyloid deposits while others did not, depending on the experimental context, presumably due to the difference in gene expression dose of hIAPP, diet condition, and/or genetic background of models examined (13, 17). Recent studies proposed that insoluble hIAPP amyloid fibrils are not toxic in β cells, but soluble toxic oligomers for hIAPP are responsible for hIAPP-induced cytotoxicity, which is collectively known as toxic oligomer hypothesis (51). In our hands, islet amyloid deposition was indeed observed in a 34-week-old high-fat diet–fed *hIAPP:Atg7$^{fl/fl}$:Cre* mouse after administration of 100 mg/kg streptozotocin (A. Hara and Y. Fujitani, unpublished observations). These observations suggest that amyloid formation is not a prerequisite for the toxic property of hIAPP, but rather one of the consequences of metabolic disorders caused by diabetes.

In the present study, despite the absence of amyloid deposits within the hIAPP-knockin pancreas, hIAPP was toxic to β cells under conditions of increased insulin demand. The toxic effects of hIAPP on β cell mass and function was exacerbated with disruption of autophagy. These observations were in agreement with the recent concept that soluble intracellular and extracellular toxic oligomers of hIAPP, rather than insoluble amyloid, may be responsible for the hIAPP-induced β cell toxicity (9, 40, 51, 52). During the design of this study, we expected that small aggregates or soluble toxic oligomers of hIAPP could be cleared by autophagy, and that inhibition of autophagy could result in accumulation of amyloid deposits. Contrary to our expectation, the results suggested that

amyloidogenesis of hIAPP is not necessarily under direct regulation of autophagic degradation.

One of the intriguing findings of this study is the presence of p62-associated putative toxic oligomers in *Atg7*-deficient β cells, which were detected by the anti-amyloid oligomer antibody A11. A11 is a conformationally specific antibody that recognizes a subset of toxic oligomers in a wide range of amyloid diseases (41, 42, 53). Importantly, islet cells immunoreactive for A11 antibody were present not only in *hIAPP:Atg7$^{fl/fl}$:Cre* mice, but also in *Atg7$^{fl/fl}$:Cre* mice (Figure 7), which indicates that toxic oligomers formed in *Atg7*-deficient β cells include those derived from amyloidogenic peptides other than hIAPP. Peptides with amyloidogenic properties that are expressed in pancreatic islets include insulin (54), α-synuclein (55), and Aβ (56, 57). Thus, possible candidates for putative toxic oligomers detected in *Atg7*-deficient β cells may include those peptides. Such a possibility warrants further investigation in the future. Interestingly, expression of hIAPP in *Atg7*-deficient β cells caused dispersion of the cytoplasmic distribution of p62 and its associated toxic oligomers (Figure 7). In this regard, genetic ablation of *p62* in *Atg7*-deficient liver and neural cells was previously reported to perturb the formation of ubiquitin-positive cytoplasmic inclusions, highlighting the critical role of p62 in this process (33). Formation of ubiquitin-positive cytoplasmic inclusions depends on the PB1 and UBA domains of p62, given that it is able to polymerize via its N-terminal PB1 domain and to recognize polyubiquitin via its C-terminal UBA domain (32, 58, 59). Therefore, one plausible function of hIAPP is inhibition of p62 function on self-aggregation. By neutralizing the function of p62, hIAPP may potentiate the toxicity of p62-associated toxic oligomers, which otherwise are sequestrated as insoluble nontoxic cytoplasmic inclusions.

In conclusion, our present results enhance the current understanding of the pathophysiological role of hIAPP during the progression of T2DM and support the significant contribution of autophagic dysfunction in the pathogenesis of this disease. We also uncovered the role of reduced autophagy in the development of β cell dysfunction and in the vulnerability of β cells to hIAPP-induced toxicity in T2DM.

Methods

Establishment of inducible Atg7 knockdown INS-1 cells. Atg7-KD INS-1 cells, a cloned cell line from parental INS-1 cells for the purpose of *Atg7* knockdown, were used as described previously (35).

Preparation of IAPP. rIAPP and hIAPP (Peptide Institute Inc.) were dissolved in DMSO and reconstituted using culture medium at a final concentration of 0.5–8.0 μM.

Human and rat prepro-IAPP adenovirus. Recombinant adenoviruses expressing hIAPP and rIAPP were prepared using the AdEasy system (60). The adenovirus titer was roughly 10^{10} infectious units/ml after treatment with the virus purification kit (VIRAPUR). We elected to use 20 and 30 MOI for INS-1 and Atg7-KD INS-1 cells, respectively. Cells were transduced with adenoviruses expressing hIAPP or rIAPP for 36, 48, or 72 hours.

Cell viability assay. INS-1 cells were plated at a density of 1×10^5 cells/well in 500 μl medium on 24-well plates. After 48 hours of culture, the medium was replaced with medium containing IAPP at the desired concentration, and incubation was continued for another 48 hours. Cells that did not stain with Trypan Blue were counted. For Atg7-KD INS-1 cells, after 36 hours of culture in tetracycline-containing medium, cells were treated with IAPP for another 36 hours.

FACS analysis. The assay was performed as described previously (61). Atg7-KD INS-1 cells were plated at a density of 5×10^4 cells/well in 24-well plates and cultured for 2 days, and incubation was continued for 3 days in tetracycline-containing medium. For cell cycle measurement, the cells were arrested with 2.8 mM glucose and 0.5% FCS for 24 hours and released for 24 hours with 22.2 mM glucose, 0.5% FCS and 200 nM insulin with or without hIAPP or rIAPP. Cells were then stained with 450 μl of 50 μg/ml propidium iodide in 0.1% Triton X-100, 4 mM sodium citrate (pH 7.2), and 450 μg/ml RNase on ice for 10 minutes, followed by the addition of 50 μl of 1.5M NaCl. Samples were analyzed on a FACSCalibur instrument (BD Biosciences). Data were processed using FlowJo (Tree Star Inc.).

Western blot analysis. Immunoblotting was performed as described previously (26). Anti-ATG7 (diluted 1:1,000; ref. 26), anti-p62 (diluted 1:1,000; Progen), anti-LC3 (diluted 1:1,000; Sigma-Aldrich), anti-GAPDH (diluted 1:1,000; Cell Signaling), or anti–β-actin (diluted 1:2,000; Sigma-Aldrich) antibodies were used.

Animal experiments. All mice were housed in specific pathogen–free barrier facilities, maintained under a 12-hour light/12-hour dark cycle, and provided standard rodent food (Oriental Yeast) or rodent food containing 60% fat (Research Diet) and water ad libitum from 8 to 20 weeks of age. We used RIP-driven Cre recombinase (*RIP-Cre*) to delete *Atg7* in a pancreatic β cell–specific manner. Generation of *Atg7$^{fl/+}$* mice was described previously (39). We crossed *RIP-Cre$^{+/-}$:Atg7$^{fl/+}$* mice with *Atg7$^{fl/+}$* mice to generate *Atg7$^{fl/fl}$* and *Atg7$^{fl/fl}$:RIP-Cre$^{+/-}$* (*Atg7$^{fl/fl}$:Cre*) mice. Mutant mice in which endogenous murine *Iapp* was genetically replaced by *hIAPP* were as described previously (17). This mouse was crossed with the *Atg7$^{fl/fl}$:Cre* mouse to generate *IAPP$^{human/human}$:Atg7$^{fl/fl}$:RIP-Cre$^{+/-}$* mice (*hIAPP:Atg7$^{fl/fl}$:Cre*), which carried homozygous *hIAPP* alleles as well as pancreatic β cell–specific autophagy deficiency. All mice were backcrossed onto C57BL/6J mice for at least 6–7 generations to minimize the contributions of genetic variation due to chimerism in the knockin.

Adjustment of body weight. The 4 groups of mice with different genotypes (approximately 40 per group) that were fed high-fat diet were subjected to body weight, food intake, and nonfasting blood glucose measurements as well as to IPGTT (Figure 3). Among these, 9–11 mice weighing 40–50 g were chosen from each group, in order to adjust the average weights of all groups to approximately 45 g, after which the data of these groups were reanalyzed (Figure 4).

Measurement of blood glucose and insulin levels. IPGTT and ITT were performed (at 20 and 21 weeks of age, respectively) as described previously (26, 62). Pancreatic islets were obtained from 5–6 mice at 23 weeks of age by collagenase digestion, as described previously (26).

Immunohistochemistry and immunostaining. Immunohistochemical analysis was carried out as described previously (26), using anti-insulin (diluted 1:2,000; Linco Research), anti-p62 (diluted 1:400; Progen), anti–amyloid oligomer (diluted 1:4,000; Millipore), anti–cleaved caspase-3 (diluted 1:400; Cell Signaling), and anti–Ki-67 (diluted 1:1,000; BD Biosciences) antibodies. Determination of β cell mass and number of intraislet cells positive for cleaved caspase-3 and Ki-67 was as described previously (26). Immunostaining was performed as described previously (63). Anti-LC3 antibody (diluted 1:500; MBL) was used for LC3 staining.

EM. EM analysis of pancreas sections was performed as previously described (62).

Statistics. All quantitative data are reported as mean ± SEM. Statistical analysis was performed using unpaired 2-tailed Student's *t* test or nonrepeated ANOVA. A *P* value less than 0.05 was considered significant.

Study approval. The protocol of animal experiments was approved by the Ethics Review Committees of Animal Experimentation of Juntendo University. All subjects gave written informed consent to the study, which was approved by the Ethics Committee of Juntendo University.

Acknowledgments

We thank T. Ueno, T. Saitoh, T. Sanke, Y. Nagai, and M. Ohsugi for valuable discussions; C.B. Newgard for INS-1 cells; N. Daimaru, E. Magoshi, K. Nakamura, H. Tsujimura, and K. Moriya for excellent technical assistance; and K. Mitani for providing human samples. We also acknowledge the support of the Mouse Facility and the Cell Imaging Core, Laboratory of Molecular and Biochemical Research, Research Support Center at Juntendo University. This work was supported by grants from the Ministry of Education, Sports and Culture of Japan (22590996 to Y. Fujitani and 23390244, 26293220, and 26111518 to H. Watada), Japan Diabetes Foundation, Daiichi-Sankyo Foundation of Life Science (to Y. Fujitani), the UBE Foundation (to H. Watada), and the project-research program of the Institute for Environmental and Gender-specific Medicine, Juntendo University (to N. Shigihara).

Address correspondence to: Yoshio Fujitani or Hirotaka Watada, Department of Metabolism and Endocrinology, Juntendo University Graduate School of Medicine, 2-1-1 Hongo, Bunkyo-ku, Tokyo 113-8421, Japan. Phone: 81.3.5802.1579; E-mail: fujitani@juntendo.ac.jp (Y. Fujitani), hwatada@juntendo.ac.jp (H. Watada).

1. Kahn SE. The relative contributions of insulin resistance and β-cell dysfunction to the pathophysiology of type 2 diabetes. *Diabetologia*. 2003;46(1):3–19.
2. Brunzell JD, et al. Relationships between fasting plasma glucose levels and insulin secretion during intravenous glucose tolerance tests. *J Clin Endocrinol Metab*. 1976;42(2):222–229.
3. Jensen CC, Cnop M, Hull RL, Fujimoto WY, Kahn SE, American Diabetes Association GSG. β-Cell function is a major contributor to oral glucose tolerance in high-risk relatives of four ethnic groups in the US. *Diabetes*. 2002;51(7):2170–2178.
4. Kloppel G, Lohr M, Habich K, Oberholzer M, Heitz PU. Islet pathology and the pathogenesis of type 1 and type 2 diabetes mellitus revisited. *Surv Synth Pathol Res*. 1985;4(2):110–125.
5. Butler AE, Janson J, Bonner-Weir S, Ritzel R, Rizza RA, Butler PC. β-Cell deficit and increased β-cell apoptosis in humans with type 2 diabetes. *Diabetes*. 2003;52(1):102–110.
6. Rahier J, Guiot Y, Goebbels RM, Sempoux C, Henquin JC. Pancreatic β-cell mass in European subjects with type 2 diabetes. *Diabetes Obes Metab*. 2008;10(suppl 4):32–42.
7. Hull RL, Westermark GT, Westermark P, Kahn SE. Islet amyloid: a critical entity in the pathogenesis of type 2 diabetes. *J Clin Endocrinol Metab*. 2004;89(8):3629–3643.
8. O'Brien TD, Butler PC, Westermark P, Johnson KH. Islet amyloid polypeptide: a review of its biology and potential roles in the pathogenesis of diabetes mellitus. *Vet Pathol*. 1993;30(4):317–332.
9. Costes S, Langen R, Gurlo T, Matveyenko AV, Butler PC. β-Cell failure in type 2 diabetes: a case of asking too much of too few? *Diabetes*. 2013;62(2):327–335.
10. Hartter E, et al. Basal and stimulated plasma levels of pancreatic amylin indicate its cosecretion with insulin in humans. *Diabetologia*. 1991;34(1):52–54.
11. Westermark P, Engstrom U, Johnson KH, Westermark GT, Betsholtz C. Islet amyloid polypeptide: pinpointing amino acid residues linked to amyloid fibril formation. *Proc Natl Acad Sci U S A*. 1990;87(13):5036–5040.
12. Betsholtz C, et al. Sequence divergence in a specific region of islet amyloid polypeptide (IAPP) explains differences in islet amyloid formation between species. *FEBS Lett*. 1989;251(1–2):261–264.
13. Matveyenko AV, Butler PC. Islet amyloid polypeptide (IAPP) transgenic rodents as models for type 2 diabetes. *ILAR J*. 2006;47(3):225–233.
14. Butler AE, Jang J, Gurlo T, Carty MD, Soeller WC, Butler PC. Diabetes due to a progressive defect in β-cell mass in rats transgenic for human islet amyloid polypeptide (HIP Rat): a new model for type 2 diabetes. *Diabetes*. 2004; 53(HIP Rat):1509–1516.
15. Janson J, et al. Spontaneous diabetes mellitus in transgenic mice expressing human islet amyloid polypeptide. *Proc Natl Acad Sci U S A*. 1996;93(14):7283–7288.
16. Verchere CB, et al. Islet amyloid formation associated with hyperglycemia in transgenic mice with pancreatic β cell expression of human islet amyloid polypeptide. *Proc Natl Acad Sci U S A*. 1996;93(8):3492–3496.
17. Hiddinga HJ, et al. Expression of wild-type and mutant S20G hIAPP in physiologic knock-in mouse models fails to induce islet amyloid formation, but induces mild glucose intolerance. *J Diabetes Investig*. 2012;3(2):138–147.
18. O'Brien TD, Butler PC, Kreutter DK, Kane LA, Eberhardt NL. Human islet amyloid polypeptide expression in COS-1 cells. A model of intracellular amyloidogenesis. *Am J Pathol*. 1995;147(3):609–616.
19. D'Alessio DA, et al. Pancreatic expression and secretion of human islet amyloid polypeptide in a transgenic mouse. *Diabetes*. 1994;43(12):1457–1461.
20. Mizushima N, Komatsu M. Autophagy: renovation of cells and tissues. *Cell*. 2011;147(4):728–741.
21. Mizushima N, Levine B, Cuervo AM, Klionsky DJ. Autophagy fights disease through cellular self-digestion. *Nature*. 2008;451(7182):1069–1075.
22. Williams A, et al. Aggregate-prone proteins are cleared from the cytosol by autophagy: therapeutic implications. *Curr Top Dev Biol*. 2006;76:89–101.
23. Yu WH, et al. Macroautophagy — a novel β-amyloid peptide-generating pathway activated in Alzheimer's disease. *J Cell Biol*. 2005;171(1):87–98.
24. Boland B, et al. Autophagy induction and autophagosome clearance in neurons: relationship to autophagic pathology in Alzheimer's disease. *J Neurosci*. 2008;28(27):6926–6937.
25. Ventruti A, Cuervo AM. Autophagy and neurodegeneration. *Curr Neurol Neurosci Rep*. 2007;7(5):443–451.
26. Ebato C, et al. Autophagy is important in islet homeostasis and compensatory increase of beta cell mass in response to high-fat diet. *Cell Metab*. 2008;8(4):325–332.
27. Jung HS, et al. Loss of autophagy diminishes pancreatic β cell mass and function with resultant hyperglycemia. *Cell Metab*. 2008;8(4):318–324.
28. Huang CJ, et al. High expression rates of human islet amyloid polypeptide induce endoplasmic reticulum stress mediated β-cell apoptosis, a characteristic of humans with type 2 but not type 1 diabetes. *Diabetes*. 2007;56(8):2016–2027.
29. Lorenzo A, Razzaboni B, Weir GC, Yankner BA. Pancreatic islet cell toxicity of amylin associated with type-2 diabetes mellitus. *Nature*. 1994;368(6473):756–760.
30. Sakagashira S, et al. S20G mutant amylin exhibits increased in vitro amyloidogenicity and increased intracellular cytotoxicity compared to wild-type amylin. *Am J Pathol*. 2000;157(6):2101–2109.
31. Morita S, et al. Autophagy protects against human islet amyloid polypeptide-associated apoptosis. *J Diabetes Investig*. 2011;2(1):48–55.
32. Komatsu M, Kageyama S, Ichimura Y. p62/SQSTM1/A170: physiology and pathology. *Pharmacol Res*. 2012;66(6):457–462.
33. Komatsu M, et al. Homeostatic levels of p62 control cytoplasmic inclusion body formation in autophagy-deficient mice. *Cell*. 2007;131(6):1149–1163.
34. Bjorkoy G, et al. p62/SQSTM1 forms protein aggregates degraded by autophagy and has a protective effect on huntingtin-induced cell death. *J Cell Biol*. 2005;171(4):603–614.
35. Abe H, et al. Exendin-4 improves β-cell function in autophagy-deficient β-cells. *Endocrinology*. 2013;154(12):4512–4524.
36. Su H, et al. Gamma-protocadherins regulate the functional integrity of hypothalamic feeding circuitry in mice. *Dev Biol*. 2010;339(1):38–50.
37. Quan W, et al. Role of hypothalamic proopi-

omelanocortin neuron autophagy in the control of appetite and leptin response. *Endocrinology*. 2012;153(4):1817–1826.
38. Gerdes J, Lemke H, Baisch H, Wacker HH, Schwab U, Stein H. Cell cycle analysis of a cell proliferation-associated human nuclear antigen defined by the monoclonal antibody Ki-67. *J Immunol*. 1984;133(4):1710–1715.
39. Komatsu M, et al. Impairment of starvation-induced and constitutive autophagy in Atg7-deficient mice. *J Cell Biol*. 2005;169(3):425–434.
40. Meier JJ, et al. Inhibition of human IAPP fibril formation does not prevent β-cell death: evidence for distinct actions of oligomers and fibrils of human IAPP. *Am J Physiol Endocrinol Metab*. 2006;291(6):E1317–E1324.
41. Glabe CG. Structural classification of toxic amyloid oligomers. *J Biol Chem*. 2008;283(44):29639–29643.
42. Kayed R, et al. Common structure of soluble amyloid oligomers implies common mechanism of pathogenesis. *Science*. 2003;300(5618):486–489.
43. Hiddinga HJ, Eberhardt NL. Intracellular amyloidogenesis by human islet amyloid polypeptide induces apoptosis in COS-1 cells. *Am J Pathol*. 1999;154(4):1077–1088.
44. Paulsson JF, Andersson A, Westermark P, Westermark GT. Intracellular amyloid-like deposits contain unprocessed pro-islet amyloid polypeptide (proIAPP) in β cells of transgenic mice overexpressing the gene for human IAPP and transplanted human islets. *Diabetologia*. 2006;49(6):1237–1246.
45. Gurlo T, et al. Evidence for proteotoxicity in β cells in type 2 diabetes: toxic islet amyloid polypeptide oligomers form intracellularly in the secretory pathway. *Am J Pathol*. 2010;176(2):861–869.
46. Ahren B, Oosterwijk C, Lips CJ, Hoppener JW. Transgenic overexpression of human islet amyloid polypeptide inhibits insulin secretion and glucose elimination after gastric glucose gavage in mice. *Diabetologia*. 1998;41(11):1374–1380.
47. Janson J, Ashley RH, Harrison D, McIntyre S, Butler PC. The mechanism of islet amyloid polypeptide toxicity is membrane disruption by intermediate-sized toxic amyloid particles. *Diabetes*. 1999;48(3):491–498.
48. Wicksteed B, et al. Conditional gene targeting in mouse pancreatic ss-Cells: analysis of ectopic Cre transgene expression in the brain. *Diabetes*. 2010;59(12):3090–3098.
49. Schmitz O, Brock B, Rungby J. Amylin agonists: a novel approach in the treatment of diabetes. *Diabetes*. 2004;53(suppl 3):S233–S238.
50. Rivera JF, et al. Human-IAPP disrupts the autophagy/lysosomal pathway in pancreatic β-cells: protective role of p62-positive cytoplasmic inclusions. *Cell Death Differ*. 2011;18(3):415–426.
51. Haataja L, Gurlo T, Huang CJ, Butler PC. Islet amyloid in type 2 diabetes, and the toxic oligomer hypothesis. *Endocr Rev*. 2008;29(3):303–316.
52. Zraika S, et al. Toxic oligomers and islet β cell death: guilty by association or convicted by circumstantial evidence? *Diabetologia*. 2010;53(6):1046–1056.
53. Laganowsky A, et al. Atomic view of a toxic amyloid small oligomer. *Science*. 2012;335(6073):1228–1231.
54. Heldt CL, Kurouski D, Sorci M, Grafeld E, Lednev IK, Belfort G. Isolating toxic insulin amyloid reactive species that lack β-sheets and have wide pH stability. *Biophys J*. 2011;100(11):2792–2800.
55. Steneberg P, et al. The type 2 diabetes-associated gene ide is required for insulin secretion and suppression of α-synuclein levels in β-cells. *Diabetes*. 2013;62(6):2004–2014.
56. Kawarabayashi T, et al. Accumulation of β-amyloid fibrils in pancreas of transgenic mice. *Neurobiol Aging*. 1996;17(2):215–222.
57. Miklossy J, et al. β amyloid and hyperphosphorylated tau deposits in the pancreas in type 2 diabetes. *Neurobiol Aging*. 2010;31(9):1503–1515.
58. Bjorkoy G, Lamark T, Johansen T. p62/SQSTM1: a missing link between protein aggregates and the autophagy machinery. *Autophagy*. 2006;2(2):138–139.
59. Itakura E, Mizushima N. p62 Targeting to the autophagosome formation site requires self-oligomerization but not LC3 binding. *J Cell Biol*. 2011;192(1):17–27.
60. He TC, Zhou S, da Costa LT, Yu J, Kinzler KW, Vogelstein B. A simplified system for generating recombinant adenoviruses. *Proc Natl Acad Sci U S A*. 1998;95(5):2509–2514.
61. Nakayama M, et al. Multiple pathways of TWEAK-induced cell death. *J Immunol*. 2002;168(2):734–743.
62. Tamaki M, et al. The diabetes-susceptible gene SLC30A8/ZnT8 regulates hepatic insulin clearance. *J Clin Invest*. 2013;123(10):4513–4524.
63. Fukunaka A, et al. Tissue nonspecific alkaline phosphatase is activated via a two-step mechanism by zinc transport complexes in the early secretory pathway. *J Biol Chem*. 2011;286(18):16363–16373.